

Highly sensitive and rapid Ochratoxin A detection via graphene field-effect transistors

Nikita Nekrasov^{a#}, Stefan Jaric^{b##*}, Dmitry Kireev^c, Aleksei V. Emelianov^a, Alexey V. Orlov^d, Ivana Gadjanski^b, Petr I. Nikitin^d, Deji Akinwande^c and Ivan Bobrinetskiy^{a,b*}

^aNational Research University of Electronic Technology, Moscow, Zelenograd, 124498, Russia, 8141147@gmail.com

^bBioSense Institute - Research and Development Institute for Information Technologies in Biosystems, University of Novi Sad, Novi Sad, 21000, Serbia

^cDepartment of Electrical and Computer Engineering, The University of Texas at Austin, Austin, TX, USA

^dProkhorov General Physics Institute of the Russian Academy of Sciences, 119991, Moscow, Russia; petr.nikitin@nsc.gpi.ru

*Corresponding author: e-mail: bobrinet@gmail.com; e-mail: sjaric@biosense.rs

these authors contributed equally

Abstract

Mycotoxins comprise a frequent type of toxins present in food and feed. The problem of mycotoxin contamination has been recently aggravated due to the increased complexity of the farm-to-fork chains, resulting in negative effects on human and animal health and, consequently, economics. The easy-to-use, on-site, on-demand, and rapid monitoring of mycotoxins in food/feed is highly desired. In this work, we report on an advanced bioelectronic mycotoxin sensor based on graphene field-effect transistors integrated on a silicon chip. A specific aptamer for Ochratoxin A (OTA) was attached to graphene through covalent bonding with the pyrene-based linker, which was deposited with an electric field stimulation to increase the surface coverage. This graphene/aptamer sensor demonstrates high sensitivity to OTA with the lowest detection limit of 1.4 pM within a response time of 10 s which is superior to any other reported aptamer-based methods.

Keywords: CVD graphene, mycotoxin, field-effect transistor, aptamer, small molecules, ionic strength

Introduction

The monitoring of small molecules (*i.e.*, of the size less than 1 kDa) has gained increasing interest in the last years in various areas of science and technology. Understanding the fundamental mechanisms of binding kinetics in molecular biology, as well as accurate and fast diagnostics of contamination in environmental, health, agriculture, and food control, demand for new methods of small molecules detection. Among the small molecules, those of high interest are drugs, antibiotics, pesticides, and toxins. Mycotoxins (MT) are of the utmost interest for health and agriculture monitoring. Mycotoxins are secondary metabolites produced by microfungi such as *Aspergillus* and *Penicillium genera* and one of the most common and dangerous contaminants in food, feed, and agricultural products [1,2]. MT can be found in a variety of foodstuffs, including cereals, dried fruit, and drinks [3]. Ochratoxin A (OTA) is one of the prevailing MT in food and feed. The standard laboratory methods like high-performance liquid chromatography-mass spectrometry (HPLC-MS) and enzyme-linked immunosorbent assay (ELISA) are traditionally used for mycotoxin detection [4]. Despite their high accuracy and sensitivity, these methods are technologically demanding in the sense of the equipment and operator qualification, which hinders their in-field application [5]. Considering the widespread of mycotoxins and their effect on economics, a fast, low-cost, and sensitive analytical tool for the on-site detection of mycotoxins is highly required [1].

Graphene field-effect transistors (GFETs) have been demonstrated as a promising platform for the rapid or real-time detection of small molecules [6,7]. One of the specific features in the use of graphene sensor for small molecule detection is the large intrinsic charges of molecules that could provide higher sensitivity in the conductivity change of the graphene channel. GFETs have previously been used for the highly sensitive detection of various antibiotics [8], small antigens [9], and small molecule drugs [10]. While sensitivity and response time are mainly defined by the physical nature of the graphene channel, selectivity is provided by the specific recognition elements, *i.e.*, bioreceptors such as enzymes, antibodies and aptamers. Aptamers are the most prospective bioreceptors that can be selected through a highly scalable process of systematic evolution of ligands by exponential enrichment (SELEX) [11]. Aptamers are oligonucleotides in a typical size range of 20 to 70 nucleic bases that form a specific three-dimensional structure during analyte capture. The oligonucleotides have intrinsic charges distributed over their backbone, and their deformation can bring charges closer to or further from the graphene surface, providing the sensing signal [8,9]. Different sensing principles based on aptamers have been demonstrated for mycotoxin detection, such as fluorescence [12], surface plasmon resonance [13], spectral-phase interferometry [14], chemiluminescence [15], and electrochemistry [16]. To the best of our knowledge, the investigation of MT effect on the electrical performance of aptamer-linked GFETs in tasks of ultra-low mycotoxin concentration analysis has not been addressed up to now. Recently, we have demonstrated a proof of concept of GFET with a liquid gate as a sensor for MT binding to aptamers immobilized on graphene [17], showing a detection limit of 10 pM and signal detection time of ~5 min. However, the reproducibility of the data is affected by graphene functionalization and aptamer attachment that greatly alter electrical properties from transistor to transistor. The use of GFETs with large area graphene channel [18] can solve this problem but with subsequent decrease of the overall sensitivity of the device.

In this work, we report on an array of optimized GFET-based aptasensors on a single chip used to detect mycotoxins that can provide better statistical data analysis generated by the sensors. Since the size of an aptamer is larger than the size of a small molecule, such as MT, the main influence on charge carriers in graphene is the transformation of the aptamer's 3D configuration due to the binding of small molecules [8]. Such advanced technology allowed us to track the processes of mycotoxin binding in real time. The novel graphene/aptamer sensors demonstrate rapid (about 10 s) and superior sensitivity to Ochratoxin A (OTA) with the limit of detection (LOD) of 1.4 pM. Furthermore, the devices were fabricated with epoxy/polydimethylsiloxane (PDMS) micro-well and tested with real wine sample drops, showing inspiring results for commercial application.

2. Material and methods

2.1 Materials and reagents

The monolayer graphene on copper foil (25 μm thick) was purchased from Grolltex (USA). Solutions of 10 $\mu\text{g}/\text{mL}$ of Ochratoxin A in acetonitrile and 0.5 $\mu\text{g}/\text{mL}$ of Aflatoxin M1 in acetonitrile were purchased from Sigma-Aldrich (USA). Anti-OTA aptamer with sequence GAT CGG GTG TGG GTG GCG TAA AGG GAG CAT CGG ACA [19] with amino-modified 5' end and purified by HPLC was purchased from Metabion AG (Germany) and Evrogen (Russia). 1-Pyrenebutyric acid N-hydroxysuccinimide ester (PBASE) was acquired from Lumiprobe RUS Ltd (Russia). Ethanolamine and tablets of phosphate-buffered saline (PBS) were acquired from Sigma-Aldrich (USA). Dimethylformamide (DMF) and isopropyl alcohol (IPA) were purchased from Component-Reactive (Russia). Dry red wine was bought in a local store.

2.2 Fabrication of the GFETs array chips

The 4-inch silicon wafers were used to produce chips (52 chips per wafer), each containing an array of GFETs using the high-throughput transfer technique described in [20,21]. In brief, the single-layer graphene was transferred onto a Si substrate with 300 nm SiO_2 layer by a wet transfer and then patterned to form graphene channels via oxygen plasma etching (300 W, 200 sccm, 10 min). Using e-beam-assisted evaporation of metals and lift-off of LOR-3B and AZ-5209-E photoresists, we deposited the 10 nm Ni and 70 nm Au metal stack. At the final step, a photostructurable resist SU-8 2002 (MicroChem) was spin-coated to form \sim 2 μm thick passivation layer. After exposure, development, and post-exposure baking, the passivation layer, covering the metal feedlines as well as a partial area ($<2 \mu\text{m}$) of graphene–metal contacts, was formed to prevent current leakage during measurements in a liquid.

To perform multiplex measurements, we wire-bonded (K&S 4524 Wire bonder) the chips on a printed circuit board (PCB). To prevent solvent leakage during measurement and save the reagents during the biosensor assembly, a 5 mm well punched in PDMS was glued by a two-component epoxy resin to the GFETs array area. The epoxy layer also protects wire bonds from unintentional damage during the chip operation.

2.3 Assembling of the GFET aptasensor

Prior to the assembling procedure, the graphene chips were treated for 5 min by low-pressure mercury lamp Svetolit-50 (power 50 W, LIT, Russia) to remove organic residuals [22]. The PBASE molecule was used as a linker for the covalent binding of aptamers. For linker immobilization on graphene by π - π stacking, we used the transverse electrical field to increase the PBASE density [23]. 4 mM PBASE solution in DMF was introduced into the PDMS well to soak graphene channels for 3 h at room temperature. Graphene channels of the GFETs were grounded while Pt wire under negative voltage with amplitude 0.3 V was inserted in DMF above the GFET array. The well was then rinsed consequently with DMF, IPA, and deionized (DI) water to remove reagent excess. 100 nM of anti-OTA aptamer dissolved in PBS solution (with pH = 7.4) was introduced into the well, and the chip on PCB was kept overnight (12 hours) in humid atmosphere to ensure aptamer binding to the PBASE linker. After rinsing several times in PBS solution to remove non-bonded aptamers, 100 mM ethanolamine solution in PBS was introduced and kept for an hour into the well to block and deactivate non-bonded reactive groups.

2.4 Aptasensor characterization and OTA detection

Optical characterization was made on optical profilometer Huvitz HRM300 (Taiwan). The presence of adsorbed PBASE on graphene surface was investigated by microRaman spectroscopy (Centaur HR, Nanoscan Technology, Russia) with a 100x objective (NA=0.9) at a 532-nm wavelength (Cobolt, Solna, Sweden) with a beam spot of 1 μm^2 and laser power of 0.5 mW.

For liquid gate measurements, we introduced the Ag/AgCl pellet electrode (Science Products GmbH) with a diameter of 1 mm in PDMS well with the analyte. For transfer curves, the drain-source voltage (V_{ds}) was set to 20 mV, and the gate voltage (V_g) was swept with 10 mV resolution. Small sweep steps provide more accurate data points. During timeseries measurements, the V_{ds} is set to 20 mV and V_g is kept at 0 V until the drain-source current (I_{ds}) was stabilized. Initial 50 μ L of blank PBS solution in a well was partly replaced by 30 μ L of OTA solution with stepwise rising concentration to prevent channel drying. The sensor's sensitivity was determined as $S=(R_0-R)/R_0$ (where R is the resistance of the GFET channel and R_0 – the resistance of the GFET channel in an OTA-free solution).

Red wine samples were diluted 10 times with PBS without any pre-treatment. To prepare spiked wine solution, the proper concentration of OTA in PBS was added to diluted wine. In this way, concentrations from 6 pM to 500 pM were obtained. The analysis was carried out in the same way as described above.

3. Results and Discussion

3.1 Device characterization

The scheme of the GFET structure and its integrated design are shown in Fig. 1. In this GFET sensor, graphene works as a channel modified by PBASE-linked aptamers. We used the recently suggested method for PBASE controlled deposition under the applied transverse electric field to increase the PBASE coverage on graphene [23].

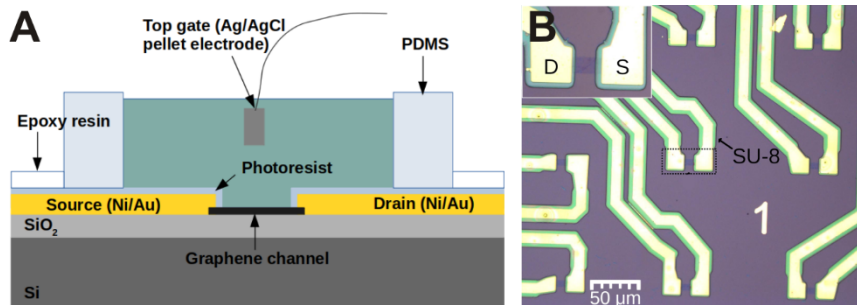


Fig. 1. Design of the sensor based on GFET. (A) A simplified scheme of a single liquid-gated GFET sensor cross-section. (B) Optical micrograph of the GFETs array on a chip with drain (D) and source (S) electrodes passivated by photoresist (SU-8) (inset: the enlarged part of graphene channel).

Fig. 2A demonstrates the final assembled device with GFET chip on PCB board. The electrical characteristics of the graphene FET after PBASE deposition and aptamer covalent binding are presented in Fig. 2B. After PBASE deposition, we observe the right shift of the Dirac point at about 75 mV due to p-type doping of graphene by a pyrene group [24]. After aptamer covalent binding to PBASE, the G-rich backbone of oligonucleotides brings the negative charge close to the graphene surface, causing weak n-type doping of graphene [25] and resulting in the left shift of the Dirac point at about 40 mV. Overall decrease in the current at all assembly steps can be associated with decreasing the number of the main charge carriers and increasing the number of the scattering centers. The latter is also causing the slope declination for both n-type and p-type branches on the transfer curves. The microRaman characterization brings more detailed information on nonlinear optical graphene properties change. There is a noticeable difference in Raman characteristics of graphene after conventional PBASE deposition and under an applied electrical field. The increase of the D band (1350 cm^{-1}) and appearance of the pyrene-related band (1628 cm^{-1}) [26] prove the PBASE deposition in both regimes. Relative intensity of this pyrene-assigned band to the G band can be used to quantify pyrene groups. The preserving G band and width of the 2D band confirms no damage of graphene that could be caused by chemical absorption (Fig. 2C). Noticeable increase in the D band with preserving 2D/G ratio (Fig. 2D) show the rise in the coverage area of PBASE when deposited under electrical field [23].

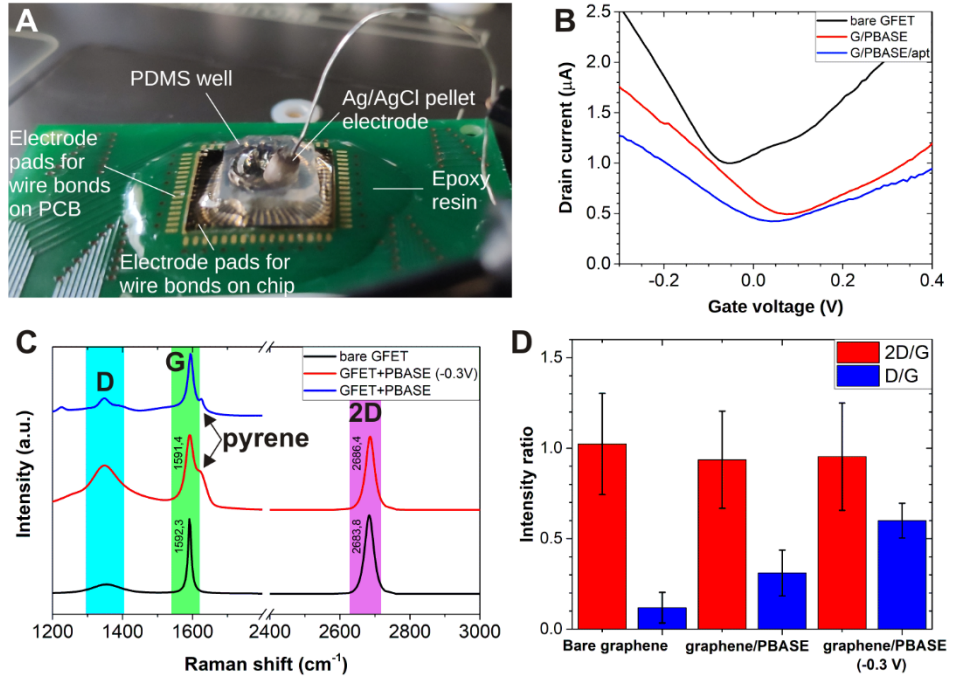


Fig. 2. Assembling the GFET aptasensor. **(A)** Photograph of the assembled sensor chip, wire-bonded on PCB with micro-well and Ag/AgCl pellet electrode. **(B)** Transfer curves of GFET at a drain voltage 20 mV for a bare GFET (black), after PBASE deposition (red), and covalent binding of aptamer (blue). **(C)** Raman spectra of bare graphene channel (black) and after PBASE deposition under -0.3V voltage applied (red) or without electrical field (blue). **(D)** The change in intensity of Raman peaks for bare graphene and after deposition of PBASE.

The main mechanism of detection for the GFET-based aptasensor is in the modulation of the channel conductance during the reconfiguration of the aptamer upon conjugation with small molecules. First, the thickness (Debye length, λ_D) of the electrical double layer (EDL) is very critical for the detection of small molecules, limiting the non-screened field-effect on the conductivity of the channel [27]. The EDL thickness is highly dependent on the ionic strength (I) of the buffer and, for example, has a value of only 0.75 nm for 1x PBS [27,28]. The aptamer reconfiguration is an important process in sensor performance because it leads to the change in distance between electrical charge in molecules and graphene. Initial configuration of an aptamer on graphene surface is still in debate suggesting either free-standing position of the aptamer [8] or π - π stacking of the backbone and aromatic bases of nucleic acids onto hexagonal carbon lattice [6,29]. The noticeable n-type doping (Fig. 2B) of graphene after aptamer deposition can confirm the π - π stacking of oligonucleotides on graphene and direct electron transfer. To provide deeper insight into the mechanism of binding of the aptamer and small molecules, we performed experiments on MT detection.

3.2 Mycotoxin detection

The liquid-gate configuration with Ag/AgCl pellet electrode and anti-OTA aptamer-modified GFET were used for OTA detection. Electrical characteristics were obtained by drop-by-drop application with partial replacement of the solutions with increasing OTA concentrations. The transfer curves were recorded for OTA solutions in PBS with different ionic strength, *i.e.*, 1x PBS buffer (Fig. 3A) and 0.1x PBS (Fig. 3B). We use multiple measurements of I-V sweeps to stabilize the EDL before OTA insertion [30]. Both the transconductance (current) increase in the hole doped region and the right shift in the Dirac point were observed with a noticeable change for lower concentration (Fig. 3C). The direction of the shift confirms the p-type doping of graphene due to reconfiguration of aptamers and decreasing the electrostatic effect on charge carriers. Shift of the Dirac point, increase of transconductance for p-type branch, and slight increase of the minimal current suggest both the change in mobility and main charge carriers

concentration in the graphene channel [6]. The electrostatic doping effect becomes more noticeable when performing experiments in 10 times diluted (0.1x) PBS (Fig. 3B). Interestingly, the transconductance has shown a nonlinear dependence on OTA concentration in 1x PBS, with current decreasing for concentrations above 100 pM. In a solution with a high ionic strength, the charges from the G-quadruplex of the aptamer can be shielded from the graphene channel by the buffer ions because of a small Debye length due to high ion concentration [6]. However, it is still possible for the mycotoxin molecules to penetrate into the EDL, doping the graphene non-specifically by direct absorption and inducing the decrease of mobility for both types of charge carriers. Increase in Debye length by dilution of the solution can significantly increase the efficiency of electrostatic gating from the aptamer, yielding the sensor's performance (Fig. 3D). The sensitivity to the OTA molecules with concentrations below 1 pM can be achieved in such a configuration (Fig. 3C). However, a small ionic strength of the buffer can limit the overall GFET-sensor application for MT detection in real samples.

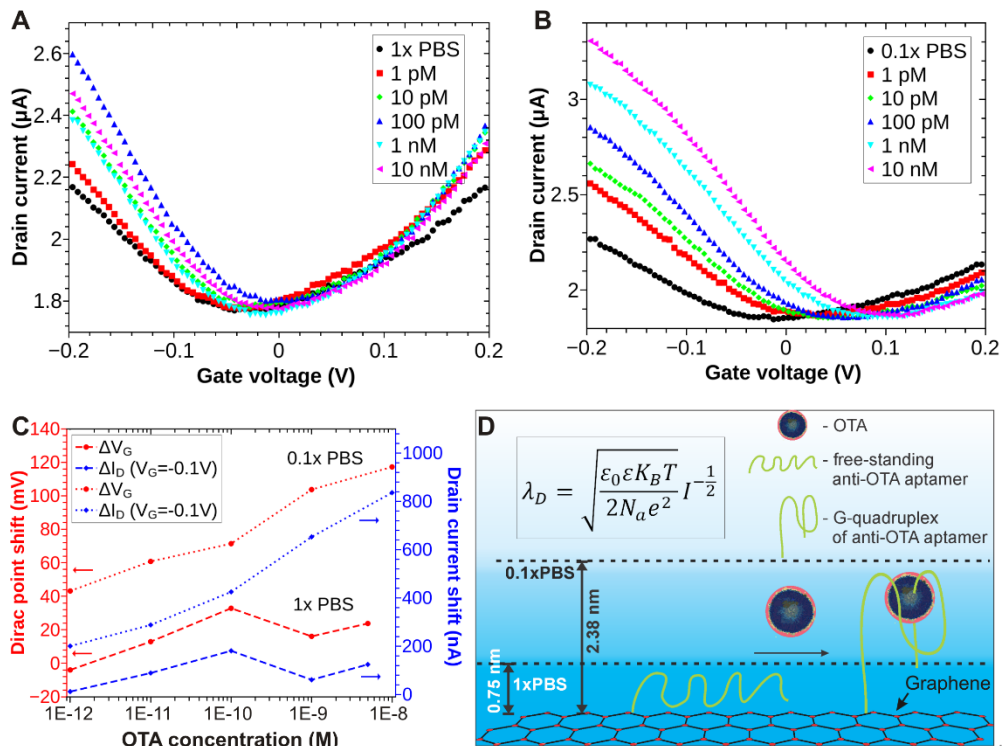


Fig. 3. Electrical characterization of the OTA sensor. (A, B) Transfer curves for different OTA concentrations in 1x PBS (A) and 0.1x PBS (B), both with $V_{ds}=100$ mV. (C) Change in the Dirac point and drain current (at $V_G=-0.1V$) for increased OTA concentrations in buffer solution with different ionic strength. (D) Hypothesized mechanism of anti-OTA aptamer target-induced reconfiguration close to graphene channels with different ionic strength. Aptamers π -stacked on graphene form G-quadruplex in the presence of OTA detracting from graphene channels, thereby increasing the transconductance and the Dirac point.

We studied the time course of aptamer-modified GFETs current change while adding the OTA solutions with different concentrations. There is a noticeable and rapid response for small concentrations of OTA (Fig. 4A). The response is saturated for concentrations above 100 pM (Fig. 4B). The rapid saturation can be explained by coverage of the receptor's sites on the surface of the graphene channel as well as by the shielding effect from the EDL layer that corresponds to the transfer curves behavior at Fig. 3A. The current increase for the aptamer-modified GFET upon OTA binding is noticeable when working in a p-doped regime and the Dirac point right shift as shown in Fig. 3A,B. To provide the control measurements, we performed similar experiments with bare non-functionalized GFET (Supporting Information: Fig. S1), and clearly no response to OTA in the concentrations up to 100 pM is visible. The noticeable resistance change for concentration higher than 4 nM (not shown) is due to the adsorption of OTA on graphene surface where phenolic moiety of the toxin can undergo π -stacking interaction [31] and results in direct doping of

graphene. The results demonstrate that the sensor can work both following the changes in the Dirac point and drain current. The drain current monitoring would provide a simple electronic tool for rapid and accurate measurements of OTA concentration in real-time in-field experiments.

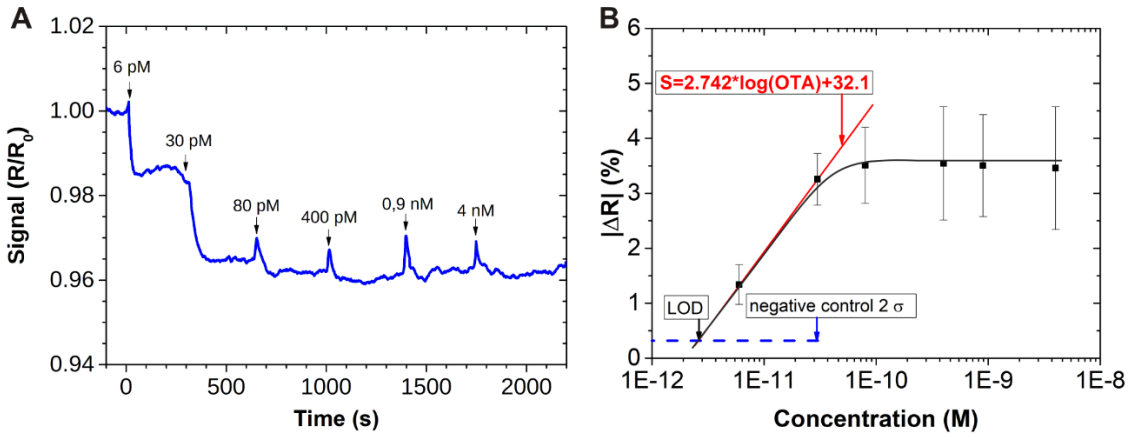


Fig. 4. Real-time measurements of OTA solutions in 1x PBS. (A) Time course of GFET array sensor response to increasing OTA concentration. (B) The calibration curve for sensitivity to the OTA based on data from five GFETs.

In general, two mechanistic concepts of GFET sensing are discussed that may take place due to aptamer conformational changes. Upon target capture, aptamer reorientation occurs in such way that a substantial portions of the negatively charged backbones are moved either closer to or further away from the sensing channels [27]. In the case of the anti-OTA aptamer, the mechanism of sensing is based on a reconfiguration of the aptamer to G-quadruplex upon binding to OTA [15,31], which is withdrawn from graphene and increase the distance from the charged aptamer and the surface, as shown in Fig. 3D. This effect can be associated with the small size of the OTA molecule (403.82 Da) compared to the longer aptamer molecules. Electrostatic gating effect in the graphene channel is very fast, yielding a short response time.

At low concentrations (1 – 100 pM), the OTA molecules are captured by the aptamer first due to their strong affinity. In response, the GFET's charge neutrality point shifts to the more positive values with OTA concentration increasing, indicating the hole doping upon the aptamer folding. Note that the maximum value of the Dirac shift for OTA in 1x PBS (Fig. 3C) is about 30 mV that is close to the initial shift due to the aptamer covalently binding to PBASE during sensor assembly. This finding supports the suggested mechanism of the partial withdrawal of the aptamer from graphene surface during the unfolding of the adsorbed state to the G-quadruplex. Some effects from OTA charge can be noticeable but only for large concentrations of OTA above 1 nM. For higher concentrations, the impact of mycotoxin is based not only on the electrostatic modulation of the charge carriers in the channel by the aptamer reconfiguration, but also on the accumulated mass/charge effect of MT molecules on aptamer-free graphene.

3.5. Analytical performance of the biosensor

Parallel experiments were carried out on an array of five GFET sensors on a single chip, and the sensor's relative response versus OTA concentration is plotted in Fig. 4B. All five devices displayed very similar properties and biosensing response, indicating excellent reproducibility. We measured the current amplitude variation of devices in the range of 6 pM to 4 nM with the linear relation to the target concentration in the range of 6 - 100 pM in 1x PBS. The noise level was calculated as relative standard deviation (RSD) of the background signal of the time course curve for negative control and equals to 0.1%. The analytical limit of detection (LOD) was determined as the intersection of the sensitivity in the linear regime and two standard deviations (2σ) of the signal of negative control [32], as shown in Fig. 4B. The calculated LOD is 1.4 pM. This detection limit is far below the tolerance level of OTA in food that is about

5 nM [33]. For calculation of response time to OTA, we used the single exponential fitting for curves presented in Fig. 5A. The time of response increases from 10 ± 3 s for 6 pM to 37 ± 13 s for 7 nM (Fig. 5B). The slowing down in the speed of change in the drain current for higher concentrations can be associated with the saturation of all receptors already for 100 pM of OTA due to the small dimensions of graphene channels. The slight variation of time for different concentrations can be associated with liquid kinetics when replacing the solution. Nevertheless, the measured response time below 60 s is still superior to the most existing mycotoxin detection methods, which typically require several minutes or up to half an hour to respond. The sensor performance in terms of speed and LOD is superior to previously reported aptasensors based on electrochemical or fluorescence methods (see Table 1).

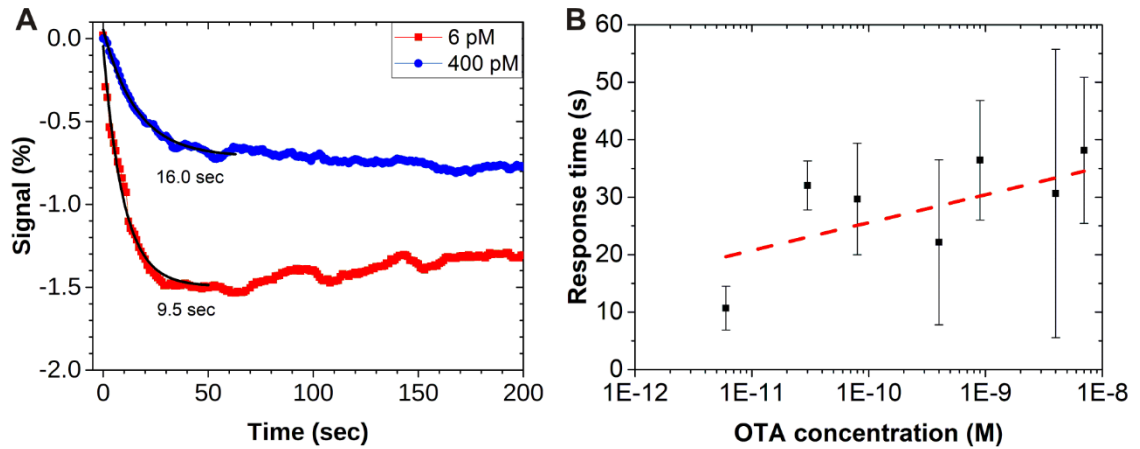


Fig. 5. Time course of resistance change of GFETs modified with the OTA aptamer. (A) Experimental data of response for 6 pM (red) and 400 pM (blue) and the single exponential fitting curves (black). (B) The response time of aptasensors array for different OTA concentrations. Red line is weighted linear fit of the data.

High sensitivity of the sensor can be explained by the increase of the binding sites for the aptamers during the electric field-supported deposition of PBASE [23]. An unprecedented sensitivity of the device is due to the high response of the graphene channel to the smallest variation of electrical charges in the surface's vicinity. Also, the antiparallel G-quadruplex aptamer topology upon OTA binding provides a more pronounced reconfiguration of the aptamer, effectively modulating the conductivity in the GFET channel. The suggested assay outperforms the recently reported approaches, making it a promising platform for proper aptamer selection and real-time kinetics investigation [34].

Table 1

Comparison of the OTA detection performances of different reported aptasensors

Detection Method	Assay with aptamer	Response Time, s	Limit of Detection, pM	Dynamic range	Ref.
FET	Graphene/PBASE	300	10	10 pM – 10 nM	[17]
fluorescence	ZnPPIX probe	-	30	-	[12]
TIRE	Glass/gold	600	30	-	[35]
CL	Signal probe/hemin	-	200	0.25 – 5 nM	[15]
EC	CdTe\graphene\Au	1800	0.2	0.5 pM – 10 nM	[36]
EC	<i>Au NPs\methylene blue</i>	1800	0.75	2.5 pM–2.5 nM	[37]
EC	Gold-dsDNA/g-CNNS	1800	73	0.2-500 nM	[16]
EC	GCE-carboxylated G-Janus particles	1800	0.01	10 fM – 10 nM	[38]

FET	Graphene/PBASE	10	1.4	5-500 pM	<i>This work</i>
CL-chemiluminescence. EC-electrochemical. ZnPPIX-Protoporphyrin IX Zinc (II). NPs - nanoparticles.					
GCE-glassy carbon electrode. CNNS - graphitic carbon nitride nanosheet. dsDNA – double-stranded DNA					

The increased speed of detection and the lower detection limit can be associated with the analyte solution injection as well. The speed of a jet flow out of the micropipette channel during experiments can be two orders of magnitude higher than the quasi-laminar flow in the pipette, reaching several meters per second [39]. We hypothesize that the high degree of turbulence present during solution injection may influence the effective mixing of the aptamer molecules. Since the aptamer molecules possess high affinity, the effective mixing may lead to rapid capturing of OTA, even in the highly diluted solutions, due to the disturbance of the dynamic balance in small molecules distribution in the solution.

3.6. Selectivity test

The selectivity of the sensors was studied on a different mycotoxin, AFM1 mycotoxin, as a nonspecific target for the OTA aptamer. The AFM1 was introduced in the sensing area through the same dynamic experimental process used for the OTA assay (Supporting Information: Fig. S2). No response was detected for the concentrations of AFM1 in the range from 1 pM to 1 nM, with only a weak response detected for AFM1 concentration higher than 1 nM, which can be explained by direct nonspecific charge transfer from MT onto graphene. Thus, the method demonstrates good selectivity.

3.7. Real samples results

Finally, to demonstrate the performance of developed sensors for the real product analysis, we spiked red wine samples with mycotoxins (Fig. 5). The high complexity of the wine matrix that consists of different chemicals both of the non-volatile nature and volatile aromas makes it analytically challenging samples. In our trials, we suggest an easy to use method that requires wine to be dissolved in a buffer only (Fig. 5A). The best agreement with the calibration curve was demonstrated for a low concentration of 6 pM that achieved $90 \pm 10\%$. Response time was estimated as 50 s for 6 pM and 74 s for 60 pM that is longer than for the PBS experiments suggesting the effect of the complex matrix of the wine, which probably limits the speed of aptamer-OTA binding. Complex ion composition of wine can also affect the EDL formation near the graphene surface [40]. This limitation on the sensor performance can be overcome by proper pH as well as in-line temperature monitoring during sensing [18]. Importantly, 6 pM concentration used for OTA in 10% wine solution in PBS translates to 60 pM of OTA in 100% wine that is two orders less than the EU legal limit for OTA in wine [33].

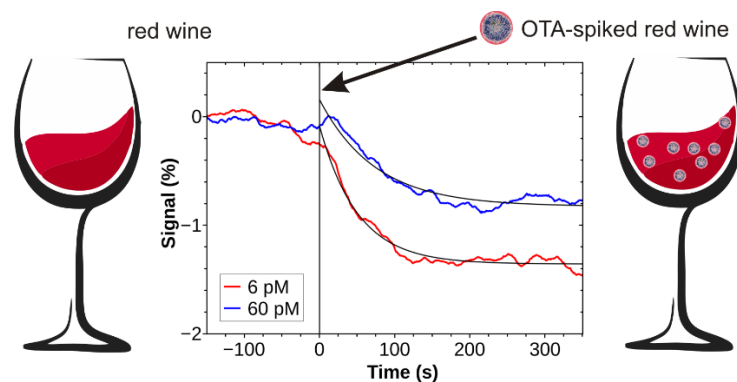


Fig. 6. Time course of resistance change of GFETs modified with the anti-OTA aptamer to wine spiked with different OTA concentrations. The zero time corresponds to the insertion of spiked wine.

4. Conclusions

A novel aptasensor based on graphene FET array for mycotoxin detection has been demonstrated. It provides accurate and rapid electrical response when the aptamer binds to the target small molecules changing its secondary configuration in the process. The response time down to 10 seconds was demonstrated in the phosphate buffer, increasing up to 50 s for real samples. The described device demonstrates unprecedented sensitivity to OTA, with a detection limit as low as 1.4 pM. The observed cross-selectivity with a different mycotoxin AFM1 makes our aptasensors a promising platform for real samples analysis. The suggested sampling method is greatly simplifying the assay preparation even for liquids with a complex matrix. Moreover, the suggested approach based on the array of GFETs could be further developed for the detection of multiple targets on a single chip after proper patterning and assembling with multiple mycotoxin-specific aptamers.

Acknowledgments

This work was supported in part by the IPANEMA project, which received funding from the European Union's Horizon 2020 research and innovation programme under grant agreement N° 872662, in part by the Russian Science Foundation under grant numbers 19-19-00401 (graphene chip development and characterization) and 19-19-00716 (monitoring the kinetics of interaction of analytes with recognition aptamers). I.G. and I.B. participated in a project that has received funding from the European Union's Horizon 2020 research and innovation programme under grant agreement N° 739570 (ANTARES). S.J. acknowledges the financial support of the Ministry of Education, Science and Technological Development of the Republic of Serbia (Grant N°. 451-03-9/2021-14/200358).

References

- [1] X. Guo, F. Wen, N. Zheng, M. Saive, M.-L. Fauconnier, J. Wang, Aptamer-Based Biosensor for Detection of Mycotoxins, *Front. Chem.* 8 (2020). doi:10.3389/fchem.2020.00195.
- [2] A.T. Mata, J.P. Ferreira, B.R. Oliveira, M.C. Batoréu, M.T. Barreto Crespo, V.J. Pereira, M.R. Bronze, Bottled water: Analysis of mycotoxins by LC–MS/MS, *Food Chem.* 176 (2015) 455–464. doi:10.1016/j.foodchem.2014.12.088.
- [3] M. Sheikh-Zeinoddin, M. Khalesi, Biological detoxification of ochratoxin A in plants and plant products, *Toxin Rev.* 38 (2019) 187–199. doi:10.1080/15569543.2018.1452264.
- [4] M.Z. Zheng, J.L. Richard, J. Binder, A Review of Rapid Methods for the Analysis of Mycotoxins, *Mycopathologia.* 161 (2006) 261–273. doi:10.1007/s11046-006-0215-6.
- [5] Y. Dong, T. Zhang, X. Lin, J. Feng, F. Luo, H. Gao, Y. Wu, R. Deng, Q. He, Graphene/aptamer probes for small molecule detection: from in vitro test to in situ imaging, *Microchim. Acta.* 187 (2020) 179. doi:10.1007/s00604-020-4128-8.
- [6] A. Béraud, M. Sauvage, C.M. Bazán, M. Tie, A. Bencherif, D. Bouilly, Graphene field-effect transistors as bioanalytical sensors: design, operation and performance, *Analyst.* 146 (2021) 403–428. doi:10.1039/D0AN01661F.
- [7] I.I. Bobrinetskiy, N.Z. Knezevic, Graphene-based biosensors for on-site detection of contaminants in food, *Anal. Methods.* 10 (2018) 5061–5070. doi:10.1039/C8AY01913D.
- [8] X. Chen, Y. Liu, X. Fang, Z. Li, H. Pu, J. Chang, J. Chen, S. Mao, Ultratrace antibiotic sensing using aptamer/graphene-based field-effect transistors, *Biosens. Bioelectron.* 126 (2019) 664–671. doi:10.1016/j.bios.2018.11.034.
- [9] Y. Kanai, Y. Ohmuro-Matsuyama, M. Tanioku, S. Ushiba, T. Ono, K. Inoue, T. Kitaguchi, M. Kimura, H. Ueda, K. Matsumoto, Graphene Field Effect Transistor-Based Immunosensor for Ultrasensitive Noncompetitive Detection of Small Antigens, *ACS Sensors.* 5 (2020) 24–28. doi:10.1021/acssensors.9b02137.

[10] S. Xu, T. Wang, G. Liu, Z. Cao, L.A. Frank, S. Jiang, C. Zhang, Z. Li, V. V. Krasitskaya, Q. Li, Y. Sha, X. Zhang, H. Liu, J. Wang, Analysis of interactions between proteins and small-molecule drugs by a biosensor based on a graphene field-effect transistor, *Sensors Actuators B Chem.* 326 (2021) 128991. doi:10.1016/j.snb.2020.128991.

[11] M.R. Dunn, R.M. Jimenez, J.C. Chaput, Analysis of aptamer discovery and technology, *Nat. Rev. Chem.* 1 (2017) 0076. doi:10.1038/s41570-017-0076.

[12] F. Liu, A. Ding, J. Zheng, J. Chen, B. Wang, A Label-Free Aptasensor for Ochratoxin a Detection Based on the Structure Switch of Aptamer, *Sensors.* 18 (2018) 1769. doi:10.3390/s18061769.

[13] Z. Zhu, M. Feng, L. Zuo, Z. Zhu, F. Wang, L. Chen, J. Li, G. Shan, S.-Z. Luo, An aptamer based surface plasmon resonance biosensor for the detection of ochratoxin A in wine and peanut oil, *Biosens. Bioelectron.* 65 (2015) 320–326. doi:10.1016/j.bios.2014.10.059.

[14] N. Nekrasov, N. Yakunina, A. V. Pushkarev, A. V. Orlov, I. Gadjanski, A. Pesquera, A. Centeno, A. Zurutuza, P.I. Nikitin, I. Bobrinetskiy, Spectral-Phase Interferometry Detection of Ochratoxin A via Aptamer-Functionalized Graphene Coated Glass, *Nanomaterials.* 11 (2021) 226. doi:10.3390/nano11010226.

[15] Y. Wang, Z. Fang, G. Ning, S. Mao, Y. Wu, S. Wu, G.-Q. Liu, G-quadruplex-bridged triple-helix aptamer probe strategy: A label-free chemiluminescence biosensor for ochratoxin A, *Sensors Actuators B Chem.* 298 (2019) 126867. doi:10.1016/j.snb.2019.126867.

[16] X. Zhu, F. Kou, H. Xu, Y. Han, G. Yang, X. Huang, W. Chen, Y. Chi, Z. Lin, Label-free ochratoxin A electrochemical aptasensor based on target-induced noncovalent assembly of peroxidase-like graphitic carbon nitride nanosheet, *Sensors Actuators B Chem.* 270 (2018) 263–269. doi:10.1016/j.snb.2018.05.048.

[17] N. Nekrasov, D. Kireev, A. Emelianov, I. Bobrinetskiy, Graphene-based sensing platform for on-chip ochratoxin a detection, *Toxins (Basel).* 11 (2019) 550. doi:10.3390/toxins11100550.

[18] I. Fakih, O. Durnan, F. Mahvash, I. Napal, A. Centeno, A. Zurutuza, V. Yargeau, T. Szkopek, Selective ion sensing with high resolution large area graphene field effect transistor arrays, *Nat. Commun.* 11 (2020) 3226. doi:10.1038/s41467-020-16979-y.

[19] J.A. Cruz-Aguado, G. Penner, Determination of Ochratoxin A with a DNA Aptamer, *J. Agric. Food Chem.* 56 (2008) 10456–10461. doi:10.1021/jf801957h.

[20] D. Kireev, D. Sarik, T. Wu, X. Xie, B. Wolfrum, A. Offenhäusser, High throughput transfer technique: Save your graphene, *Carbon N. Y.* 107 (2016) 319–324. doi:10.1016/j.carbon.2016.05.058.

[21] A. V. Emelianov, D. Kireev, A. Offenhäusser, N. Otero, P.M. Romero, I.I. Bobrinetskiy, Thermoelectrically Driven Photocurrent Generation in Femtosecond Laser Patterned Graphene Junctions, *ACS Photonics.* 5 (2018) 3107–3115. doi:10.1021/acsphotonics.8b00350.

[22] A.V. Emelianov, D. Kireev, D.D. Levin, I.I. Bobrinetskiy, The effect of ultraviolet light on structural properties of exfoliated and CVD graphene, *Appl. Phys. Lett.* 109 (2016). doi:10.1063/1.4965975.

[23] Z. Hao, Y. Pan, C. Huang, Z. Wang, Q. Lin, X. Zhao, S. Liu, Modulating the Linker Immobilization Density on Aptameric Graphene Field Effect Transistors Using an Electric Field, *ACS Sensors.* 5 (2020) 2503–2513. doi:10.1021/acssensors.0c00752.

[24] G. Wu, X. Tang, M. Meyyappan, K.W.C. Lai, Doping effects of surface functionalization on graphene with aromatic molecule and organic solvents, *Appl. Surf. Sci.* 425 (2017) 713–721. doi:10.1016/j.apsusc.2017.07.048.

[25] E. Danielson, V.A. Sontakke, A.J. Porkovich, Z. Wang, P. Kumar, Z. Ziadi, Y. Yokobayashi, M. Sowwan, Graphene based field-effect transistor biosensors functionalized using gas-phase

synthesized gold nanoparticles, *Sensors Actuators B Chem.* 320 (2020) 128432. doi:10.1016/j.snb.2020.128432.

[26] Y. Liu, L. Yuan, M. Yang, Y. Zheng, L. Li, L. Gao, N. Nerngchamnong, C.T. Nai, C.S.S. Sangeeth, Y.P. Feng, C.A. Nijhuis, K.P. Loh, Giant enhancement in vertical conductivity of stacked CVD graphene sheets by self-assembled molecular layers, *Nat. Commun.* 5 (2014) 5461. doi:10.1038/ncomms6461.

[27] N. Nakatsuka, K.-A. Yang, J.M. Abendroth, K.M. Cheung, X. Xu, H. Yang, C. Zhao, B. Zhu, Y.S. Rim, Y. Yang, P.S. Weiss, M.N. Stojanović, A.M. Andrews, Aptamer–field-effect transistors overcome Debye length limitations for small-molecule sensing, *Science* (80-.). 362 (2018) 319–324. doi:10.1126/science.aa06750.

[28] I.-Y. Sohn, D.-J. Kim, J.-H. Jung, O.J. Yoon, T. Nguyen Thanh, T. Tran Quang, N.-E. Lee, pH sensing characteristics and biosensing application of solution-gated reduced graphene oxide field-effect transistors, *Biosens. Bioelectron.* 45 (2013) 70–76. doi:10.1016/j.bios.2013.01.051.

[29] H. Wang, T. Chen, S. Wu, X. Chu, R. Yu, A novel biosensing strategy for screening G-quadruplex ligands based on graphene oxide sheets, *Biosens. Bioelectron.* 34 (2012) 88–93. doi:10.1016/j.bios.2012.01.023.

[30] W. Fu, L. Feng, G. Panaitov, D. Kireev, D. Mayer, A. Offenhäusser, H.-J. Krause, Biosensing near the neutrality point of graphene, *Sci. Adv.* 3 (2017) e1701247. doi:10.1126/sciadv.1701247.

[31] K.L. Fadock, R.A. Manderville, DNA Aptamer–Target Binding Motif Revealed Using a Fluorescent Guanine Probe: Implications for Food Toxin Detection, *ACS Omega.* 2 (2017) 4955–4963. doi:10.1021/acsomega.7b00782.

[32] A. V. Orlov, A.G. Burenin, N.G. Massarskaya, A. V. Betin, M.P. Nikitin, P.I. Nikitin, Highly reproducible and sensitive detection of mycotoxins by label-free biosensors, *Sensors Actuators B Chem.* 246 (2017) 1080–1084. doi:10.1016/j.snb.2016.12.071.

[33] J. Gil-Serna, C. Vázquez, M. González-Jaén, B. Patiño, Wine Contamination with Ochratoxins: A Review, *Beverages.* 4 (2018) 6. doi:10.3390/beverages4010006.

[34] V.C.F. dos Santos, N.B.F. Almeida, T.A.S.L. de Sousa, E.N.D. Araujo, A.S.R. de Andrade, F. Plentz, Real-time PCR for direct aptamer quantification on functionalized graphene surfaces, *Sci. Rep.* 9 (2019) 19311. doi:10.1038/s41598-019-55892-3.

[35] A. Al Rubaye, A. Nabok, G. Catanante, J.-L. Marty, E. Takacs, A. Szekacs, Detection of ochratoxin A in aptamer assay using total internal reflection ellipsometry, *Sensors Actuators B Chem.* 263 (2018) 248–251. doi:10.1016/j.snb.2018.01.220.

[36] N. Hao, L. Jiang, J. Qian, K. Wang, Ultrasensitive electrochemical Ochratoxin A aptasensor based on CdTe quantum dots functionalized graphene/Au nanocomposites and magnetic separation, *J. Electroanal. Chem.* 781 (2016) 332–338. doi:10.1016/j.jelechem.2016.09.053.

[37] X. Yang, J. Qian, L. Jiang, Y. Yan, K. Wang, Q. Liu, K. Wang, Ultrasensitive electrochemical aptasensor for ochratoxin A based on two-level cascaded signal amplification strategy, *Bioelectrochemistry.* 96 (2014) 7–13. doi:10.1016/j.bioelechem.2013.11.006.

[38] Y.-J. Yang, Y. Zhou, Y. Xing, G.-M. Zhang, Y. Zhang, C.-H. Zhang, P. Lei, C. Dong, X. Deng, Y. He, S. Shuang, A Label-free aptasensor based on Aptamer/NH₂ Janus particles for ultrasensitive electrochemical detection of Ochratoxin A, *Talanta.* 199 (2019) 310–316. doi:10.1016/j.talanta.2019.02.015.

[39] M. Priebe, S. Kalbfleisch, M. Tolkiehn, S. Köster, B. Abel, R.J. Davies, T. Salditt, Orientation of biomolecular assemblies in a microfluidic jet, *New J. Phys.* 12 (2010) 043056. doi:10.1088/1367-2630/12/4/043056.

[40] M.H. Lee, B.J. Kim, K.H. Lee, I.-S. Shin, W. Huh, J.H. Cho, M.S. Kang, Apparent pH sensitivity of solution-gated graphene transistors, *Nanoscale*. 7 (2015) 7540–7544. doi:10.1039/C5NR00414D.

Supporting Information

Highly sensitive and rapid Ochratoxin A detection via graphene field-effect transistors

Nikita Nekrasov^a#, Stefan Jaric^{b##*}, Dmitry Kireev^c, Aleksei V. Emelianov^a, Alexey V. Orlov^d, Ivana Gadjanski^b, Petr I. Nikitin^d, Deji Akinwande^c and Ivan Bobrinetskiy^{a,b*}

^aNational Research University of Electronic Technology, Moscow, Zelenograd, 124498, Russia, 8141147@gmail.com

^bBioSense Institute - Research and Development Institute for Information Technologies in Biosystems, University of Novi Sad, Novi Sad, 21000, Serbia

^cDepartment of Electrical and Computer Engineering, The University of Texas at Austin, Austin, TX, USA

^dProkhorov General Physics Institute of the Russian Academy of Sciences, 119991, Moscow, Russia; petr.nikitin@nsc.gpi.ru

*Corresponding author: e-mail: bobrinet@gmail.com; e-mail: sjaric@biosense.rs

these authors contributed equally

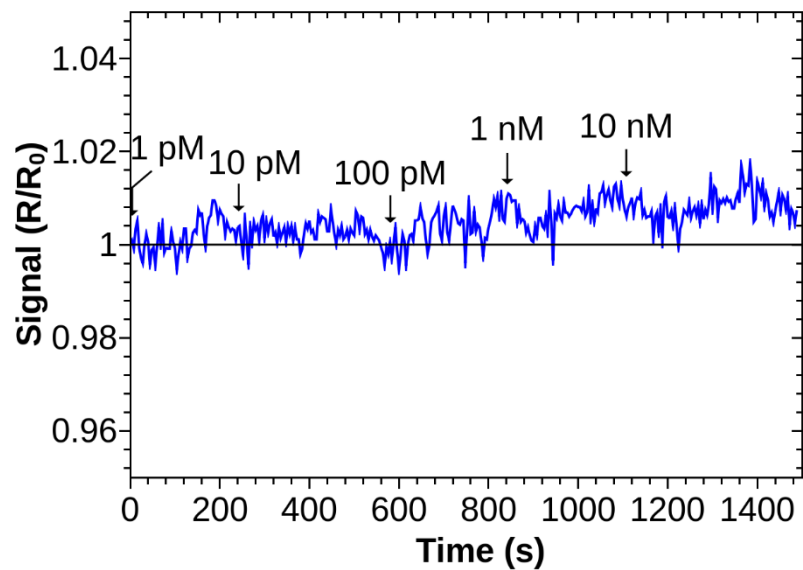


Fig. S1. Time course for bare (non-functionalized) GFET for different OTA concentrations.

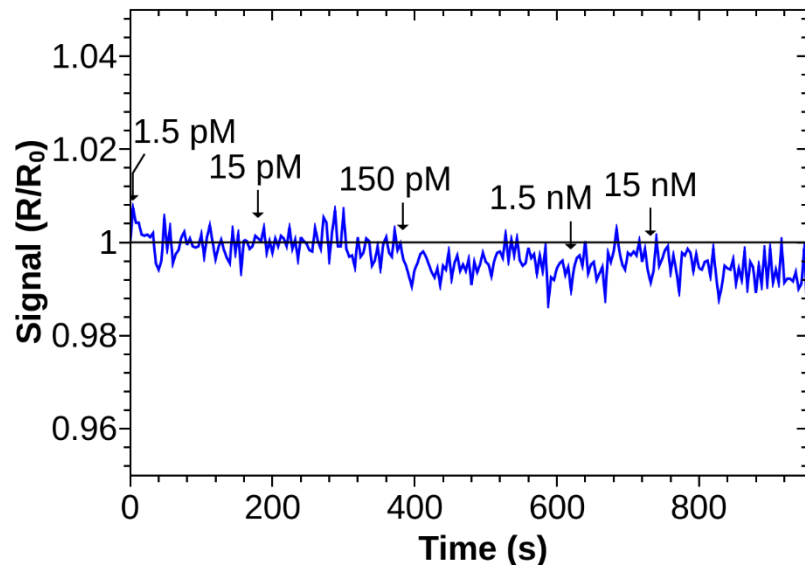


Fig. S2. Control experiments. Response time course for anti-OTA aptamer-modified GFET when different concentrations of AFM1 in 1x PBS are applied.